Clays and Clay Minerals, Vol. 35, No. 3, 196–202, 1987.

NATROALUNITE IN A LATERITE PROFILE OVER DECCAN TRAP BASALTS AT MATANUMAD, KUTCH, INDIA

D. V. CHITALE AND N. GÜVEN

Department of Geoscience, Texas Tech University
Lubbock, Texas 79409

Abstract—An end-member natroalunite of composition $(K_{0.04}Na_{0.96})(Al_{2.98}Fe_{0.02})(SO_4)_2(OH)_6$ occurs in saprolitic clays in a laterite profile developed over Deccan Trap basalts at Matanumad in the Kutch region of Gujarath state, India. Pseudocubic natroalunite crystals, ranging from 0.5 to 1 μm in size, have replaced pseudohexagonal, 2-μm-size platelets of kaolinite. The reverse reaction (kaolinization of natroalunite) has also been observed in the laterites and bauxites immediately adjacent to the saprolite. The kaolinite crystallites that replaced natroalunite occur as a mosaic of anhedral platelets that range in size from 0.1 to 0.3 μm. The formation of natroalunite at Matanumad postdates the laterization of the basalts. It is related to the post-diagenetic formation of sulfuric acid-rich solutions by the oxidation of pyrite in the Eocene-Oligocene black shales of the Matanumad basin. The kaolinitic clays at the top of the saprolite zone have been intensely altered by the acidic solutions, leading to a high concentration of natroalunite.

Key Words—Alunite, Kaolinite, Laterite, Natroalunite, Oxidation, Saprolite.

INTRODUCTION

Alunite-natroalunite minerals form a solid solution series having the general chemical composition $(K,Na)Al_3(SO_4)_2(OH)_6$. The alkali ions are in 12-fold coordination between the sheets of aluminum octahedra that share OH ligands. By definition, natroalunite represents the members of the group in which Na > K in the structure, whereas alunite refers to members in which K > Na. Partial substitution of alkali ions by H_3O^+ was synthetically accomplished by Parker (1962). A calcium-rich variety named minamiite was recently reported by Ossaka *et al.* (1982); this mineral has the composition $(Na_{0.36}K_{0.10}Ca_{0.27})Al_3(SO_4)_2(OH)_6$. The distribution of alkali ions in natural and synthetic alunite-natroalunite series was studied by Parker (1962) and Cunningham and Hall (1976). The K-rich alunites are common in nature suggesting that K^+ is preferred over Na^+ in the crystal structure of this compound. An end-member natroalunite with an alkali composition of $(Na_{0.99}K_{0.01})$ was reported by Moss (1958).

The following report describes another end-member natroalunite having an alkali composition of $(Na_{0.96}K_{0.04})$ from a laterite profile developed over Deccan Trap basalts at Matanumad, Kutch, India. The occurrence, mineralogy, and the geological conditions of formation of this end-member natroalunite are described below.

LATERITE PROFILE AT MATANUMAD

A laterite profile containing a large concentration of natroalunite is exposed at Matanumad, 110 km northwest of Bhuj, in the Kutch region of Gujarath state, India (Figure 1). The geology of the laterites and bauxites of Kutch region was recently studied by Shukla *et al.* (1983) and Das Gupta (1984). The laterites at Matanumad are part of a laterite belt that parallels the Kutch coast in western India and extends from Anjar on the east to Lakhpat on the west. Several low-lying hills near Matanumad are capped by laterites. Laterite outcrops in a hill about 0.5 km east-northeast of the Public Welfare Department's guest house were studied in this investigation.

Figure 2 shows a typical succession of rock types in the laterite profile at Matanumad. Here, a 20-m-high hill is capped by a 3-m-thick laterite crust that ranges in color from deep red at the top through brick red in the intermediate zone, to purple-brown at its lower boundary. The laterite is hard and massive in the upper 1 m of the crust and is relatively more brittle in the lower 2-m portion. Locally, pockets and lenses of red or light-purple bauxite are present within the laterite crust, ranging in thickness from 0.5 to 1.0 m.

The laterite and bauxite grade downward into a zone of saprolitic clay that ranges in thickness from 2 to 4 m. The clay exhibits different colors, e.g., gray, pinkish white, creamy white, purple, and yellow. The most striking feature of the saprolite zone is the common occurrence of distinctly colored clay strata. In general, creamy white clays are successively underlain by purple and yellow clays. Such horizons are individually about 1 m thick and are continuous over the entire extent (0.5 km) of the laterite outcrops in the hill. The saprolite zone merges downward into a zone of spheroidally weathered basalt. Locally, spheroidal boulders of clay display a complete transformation of basalt spheroids to saprolitic clay *in situ*.

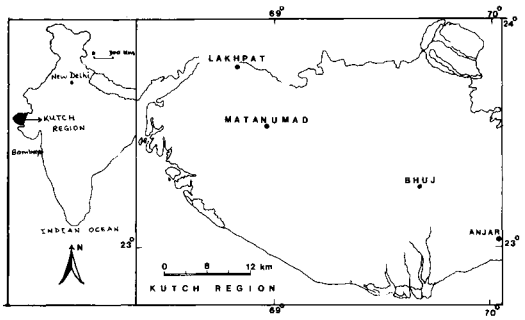

Figure 1. Sketch map showing location of Matanumad in the Kutch region of India.

MATERIALS AND METHODS

Twenty-five samples of laterite, bauxite, and saprolitic clay were hand-picked from the laterite profile described above to represent the vertical and lateral variations in color, texture, and physical appearance of the rocks.

Mineral composition of the various rocks was determined by X-ray powder diffraction analysis (XRD). Both random powder mounts and oriented specimens were examined with a Philips diffractometer using CuKα radiation. The micromorphology of the rocks was examined by scanning (SEM) and transmission (TEM) electron microscopy. The elemental composition of various minerals in the rocks was determined by means of energy-dispersive X-ray (EDX) analysis. The electron microscopic and the EDX analyses were conducted on a JEM 100-CX electron microscope equipped with an EG & G ORTEC EEDS II X-ray analyzer. The samples for SEM were prepared from freshly broken surfaces of the rocks. The TEM specimens were prepared from the clay fractions (<2 μm) of the rocks. A natroalunite sample (M6) with no impurities detectable by XRD was chemically analyzed with inductively coupled plasma-atomic emission spectroscopy by Robert I. Botto of Exxon Research & Engineering Company, Baytown, Texas.

RESULTS AND DISCUSSION

The mineral composition of different samples collected from the laterite profile in Figure 2 is summarized in Table 1. Although the minerals were primarily identified by XRD, some minerals could be detected only with TEM.

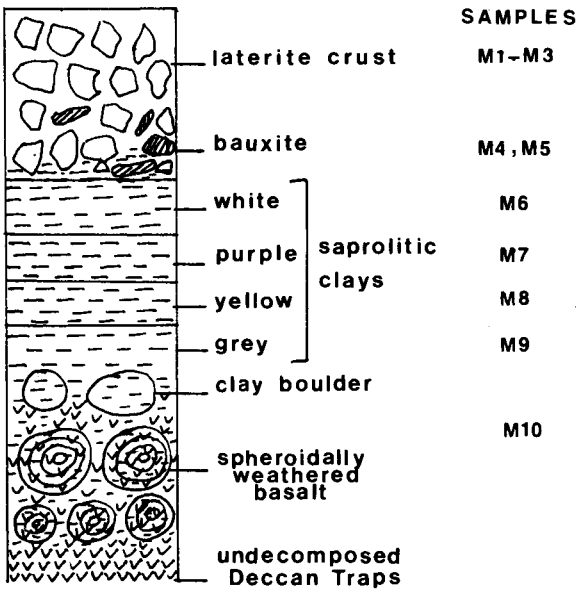

Figure 2. A schematic representation (not to scale) of the laterite profile at Matanumad.

Natroalunite is the predominant mineral in the saprolitic clay horizon; kaolinite is present in subordinate amounts (Table 1, samples M6–M9). Natroalunite and kaolinite were identified on the basis of XRD patterns. The XRD data for natroalunite in Table 2 agree closely with the indexed data for natroalunite by Parker (1962). Also, the *a* and the *c* lattice parameters of natroalunite were calculated using the $22\bar{4}0$ and 0009 reflections, respectively. These unit-cell parameters of natroalunite are compared with those of the end-member alunite, the end-member natroalunite, and Na-jarosite (see below). Crystal chemical studies of the alunite group minerals by Okada *et al.* (1982), Menchetti and Sabelli (1976), Brophy *et al.* (1962), and Parker (1962) convincingly demonstrated that the *c* parameter is highly sensitive to the substitutions in alkali positions, whereas the *a* parameter is affected by octahedral (Al,Fe) substitutions. The *c* parameter of the natroalunite from Matanumad is close to that of the end-member natroalunite of Parker (1962). The slightly larger *a* parameter suggests the presence of a small amount of Fe^{3+} in the structure.

The chemical analysis of the bulk sample containing no crystalline impurities detectable by XRD is given

		a (Å)	*c* (Å)
Natroalunite	(this study)	6.992 (7)	16.725 (7)
Natroalunite	$(Na_{0.99}K_{0.01})Al_3(SO_4)_2(OH)_6$ (Parker, 1962)	6.983	16.699
Alunite	$(Na_{0.03}K_{0.97})Al_3(SO_4)_2(OH)_6$ (Parker, 1962)	6.981	17.34
Na-jarosite	$NaFe_3(SO_4)_2(OH)_6$ (Menchetti and Sabelli, 1976)	7.327	16.634

https://doi.org/10.1346/CCMN.1987.0350305 Published online by Cambridge University Press

Table 1. Distribution of minerals in the Matanumad, India, laterite profile.

Sample	Depth (m)	Brief description of the sample	Mineral composition[1]
M1	0.0–1.5	hard, massive, deep red laterite	hm, nt, kt, an, gt[2]
M2	1.0–2.0	massive, reddish-brown laterite	hm, nt, gt, kt
M3	1.5–2.5	soft, brittle, brown laterite	gt, hm, kt, an
M4	1.5–3.0	light purple bauxite	gb, kt, hm, gt, an
M5	2.0–3.5	clayey bauxite	kt, gb, an, hm, gt[2]
M6	3.0–4.0	creamy white saprolitic clay	nt, kt[3]
M7	4.0–5.0	purple saprolitic clay	nt, kt, hm, gt,[2] hl[3]
M8	5.0–5.5	yellow saprolitic clay	nt, kt, hm, hl[3]
M9	5.5–6.5	buff-gray saprolitic clay	nt, kt, an, gt, hl[3]
M10	6.5–7.0	clays in and just out of the outermost exfoliated layer of basalt	kt, hm,[2] gt,[2] an,[2] hl[3]

[1] Minerals identified by X-ray powder diffraction and arranged in the decreasing order of abundance: nt = natroalunite; kt = kaolinite; an = anatase; gt = goethite; gb = gibbsite; hl = halloysite.

[2] Present in trace amounts.

[3] Detected only by means of scanning or transmission electron microscopy; present in traces.

in Table 3. The SO_3-content of 37.75% indicates that natroalunite makes up 94% of the sample. The silica (0.09%) was assigned to kaolinite that was detected by electron microscopy. After correcting alumina for kaolinite, the chemical composition of the natroalunite was calculated as:

$$(Na_{0.96}K_{0.04})(Al_{2.98}Fe^{3+}{}_{0.02})(SO_4)_2(OH)_6.$$

The unit-cell parameters obtained from the XRD data

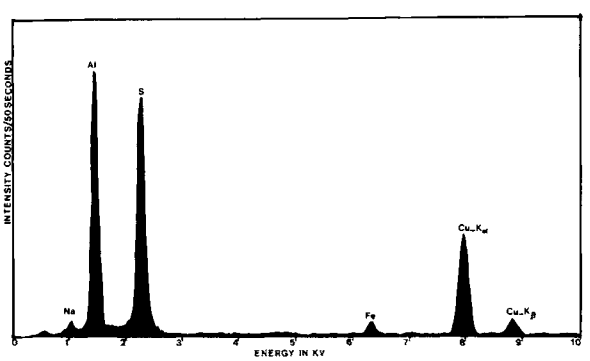

Figure 3. Characteristic X-ray spectra representing the chemical composition of a natroalunite crystallite in Figure 6 (CuKα and CuKβ lines belong to the sample holder).

Table 2. X-ray powder diffraction data for natroalunite in the creamy white saprolitic clay (sample M6), Matanumad, Kutch, India.

d (Å)	I	*hkil*[1]
5.68	2	$10\bar{1}1$
5.55	2	0003
4.90	55	$01\bar{1}2$
3.49	23	$11\bar{2}0$
3.44	1	$10\bar{1}4$
2.969	60	$02\bar{2}1$
2.960	100	$11\bar{2}3$
2.929	12	$01\bar{1}5$
2.790	7	0006
2.449	2	$02\bar{2}4$
2.242	2	$20\bar{2}5$
2.221	39	$10\bar{1}7$
1.896	41	$30\bar{3}3$
1.875	2	$02\bar{2}7$
1.857	5	0009
1.747	32	$22\bar{4}0$
1.645	7	$11\bar{2}9$
1.558	4	$13\bar{4}4$
1.542	6	$12\bar{3}8$
1.500	2	$31\bar{4}5$
1.480	8	$22\bar{4}6$
1.463	20	$02\bar{2}10$

[1] The *hkil* indices were assigned according to Parker (1962).

and the characteristic X-ray spectra obtained from the individual crystallites of natroalunite confirm the above chemical composition. No K-line was detected in the X-ray spectrum of the natroalunite (Figure 3). Potassium must therefore be below the detection level; Al and S were the main spectral lines observed along with

Table 3. Chemical composition of the bulk natroalunite sample (M6), on moisture-free basis.

Oxide	Wt. %
Al_2O_3	35.66
Fe_2O_3	1.10
Na_2O	6.12
K_2O	0.39
SO_3	37.75
SiO_2	0.09
TiO_2	0.10
MnO	0.01
CaO	0.06
MgO	0.01
Total[1]	81.29

[1] Total reflects the sum of the oxides and SO_3; H_2O+ was not determined.

→

Figure 4. Scanning electron micrograph showing authigenic growth of natroalunite crystals (N) in the micropores within a vermicular stack of kaolinite platelets.

https://doi.org/10.1346/CCMN.1987.0350305 Published online by Cambridge University Press

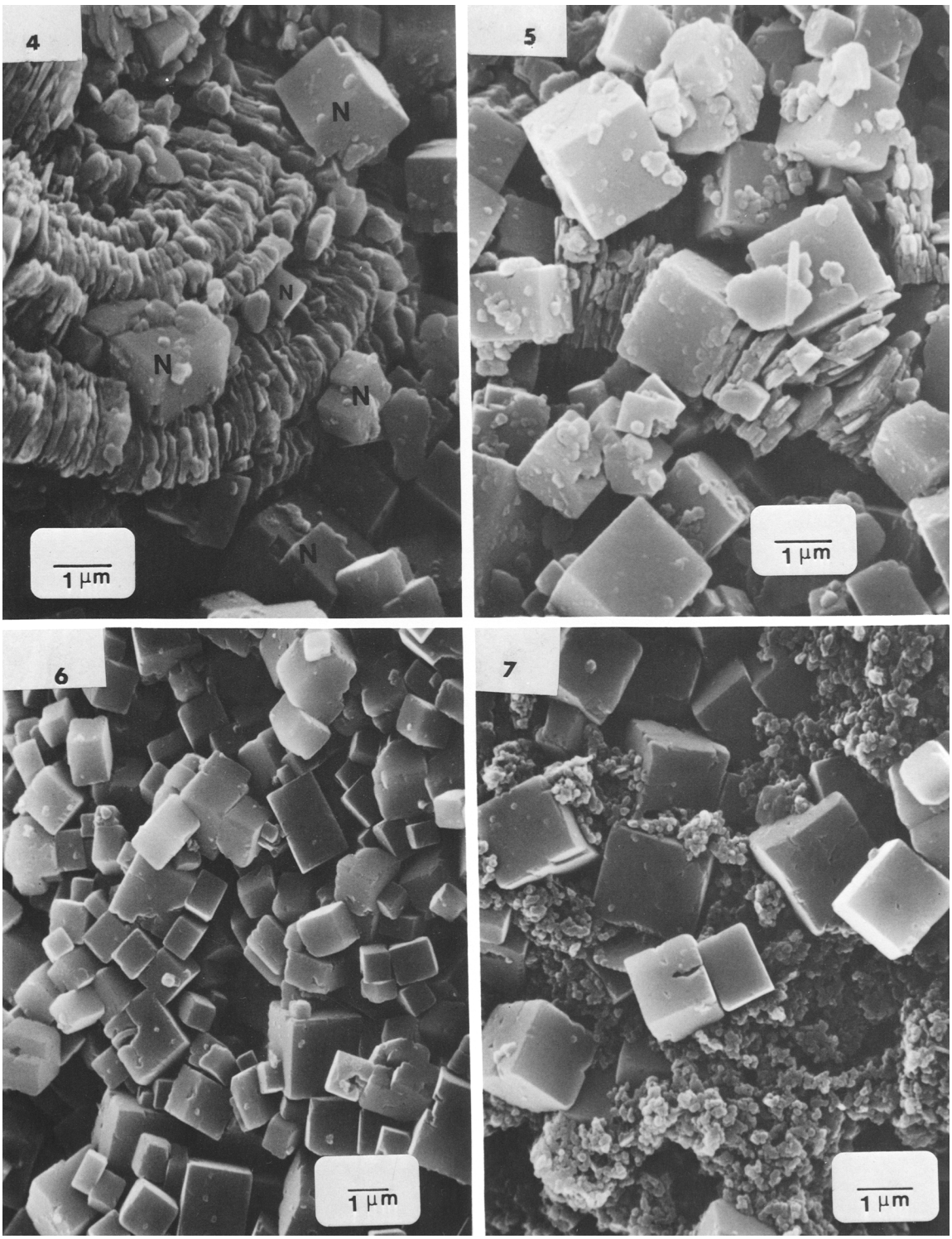

Figure 5. Scanning electron micrograph showing a more advanced stage of natroalunization.

Figure 6. Scanning electron micrograph of a completely natroalunized saprolite showing aggregates of natroalunite crystals without relict kaolinite.

Figure 7. Scanning electron micrograph showing submicrometer-size anhedral crystallites of kaolinite formed interstitially in natroalunite.

https://doi.org/10.1346/CCMN.1987.0350305 Published online by Cambridge University Press

a weak but distinct line of Fe. The latter line suggests a small amount of Fe^{3+} substituting for Al in octahedral positions.

The relative abundance of natroalunite with respect to kaolinite steadily increases upwards within the saprolite horizon (Table 1). The top layer of white saprolitic clay consists almost entirely of natroalunite. Figure 4 represents the initial stage of natroalunization, with pseudocubic-rhombohedral crystallites of natroalunite occurring in and around the vermicular stacks of kaolinite platelets. The natroalunite crystallites range in size from 0.6 to 1.0 μm, whereas kaolinite platelets of about 2.0 μm form vermicular stacks as thick as 10–20 μm. What appears to be a more advanced stage of natroalunitization is illustrated in Figure 5. A completely natroalunitized saprolite containing no kaolinite relicts consists of pseudocubes and rhombohedra of natroalunite ranging in size from 0.5 to 1.5 μm (Figure 6). A typical X-ray spectrum of a natroalunite rhomb is given in Figure 3 (*vide supra*).

The relative abundance of natroalunite sharply decreases in the laterites and bauxites overlying the saprolitic clays (Table 1 and Figure 2; samples M5 and M1). The bauxites consist chiefly of gibbsite and kaolinite, with minor proportions of anatase, hematite, and goethite. In the laterites adjacent to the bauxites, goethite and hematite predominate, and kaolinite and anatase are present in subordinate amounts. Natroalunite is altogether absent in the bauxites adjacent to the white saprolitic clay, as well as in the laterites immediately around bauxites (samples M3–M5). SEM investigations of the bauxites and laterites suggest that the initial stage of kaolinization was marked by precipitation of extremely minute (<1000 Å) anhedral crystals of kaolinite in the voids between the natroalunite crystals (Figure 7). The X-ray spectra obtained from these crystallites show a spectral intensity ratio of about 0.8 for Al/Si lines, typical of kaolinite. An advanced stage of kaolinization is shown in Figure 8. Here, the pseudocubic crystals of natroalunite appear to have been attacked from all sides, and the kaolinization proceeded inwards. The newly formed kaolinite platelets are anhedral and range in size from 0.1 to 0.3 μm. An apparently complete replacement of natroalunite by kaolinite is shown in Figure 9 where some of the particles still exhibit pseudocubic morphology but the X-ray spectra show only Al- and Si-lines having a spectral intensity ratio similar to that of kaolinite. The kaolinite crystals that formed as the replacement of natroalunite occur as a random mosaic of anhedral platelets, about 0.1 μm in size. The morphological and textural features of this kaolinite are totally different from those of the vermicular stacks of pseudo-hexagonal platelets of kaolinite in the saprolite (Figure 4).

The evidence for the formation of gibbsite at the expense of natroalunite is not as obvious as for the kaolinization of natroalunite; however, much of the gibbsite in the bauxites occurs as anhedral platelets ranging in size from 0.5 to 1 μm (Figure 10). The identity of gibbsite crystals in Figure 10 was established by the EDX spectra that showed only Al-lines.

In the uppermost 2 m of the laterite crust, natroalunite and kaolinite are disseminated with kaolinite in subordinate quantities. Here, hematite and goethite are the predominant minerals (Table 1, samples M1–M3). Natroalunite occurs as typical pseudocubic crystals in a compact matrix of microcrystalline hematite-goethite intergrowths (Figure 11). No genetic relationship between natroalunite and the hematite-goethite aggregates is apparent.

FORMATION OF NATROALUNITE AT MATANUMAD

According to the geologic history of the Kutch region as proposed by Biswas (1971) and Shukla *et al.* (1983), the laterization in the Matanumad basin took place in the Paleocene. Later, during the Middle Eocene, the Matanumad basin was submerged, and lignites and black shales rich in pyrite were deposited. The shales and lignites were eroded following the post-Pliocene uplift, and the laterites were exposed again as capping the basalts. None of the horizons within the laterite contain sulfide minerals. Therefore, natroalunization probably occurred after the deposition of pyrite-containing shales and lignites over the laterites. The oxidation of pyrite is the most probable source of sulfate-rich solutions that may also have leached Na^+ from sodium-bearing minerals in the sediments deposited over laterites at Matanumad. The reaction of these sulfate- and sodium-rich solutions with kaolinite in the saprolites below the porous laterites may have been the principal process for the natroalunitization. This process can be represented by the following equation for the kaolinite-natroalunite equilibrium and is analogous to the kaolinite-alunite equilibrium described by Raymahashay (1968), Hemley *et al.* (1969), and Lindsay (1979):

→

Figure 8. Scanning electron micrograph showing apparent replacement of natroalunite by kaolinite.

Figure 9. Scanning electron micrograph showing massive aggregate of anhedral crystallites of kaolinite; some kaolinite aggregates appear to have retained the original pseudocubic morphology of natroalunite.

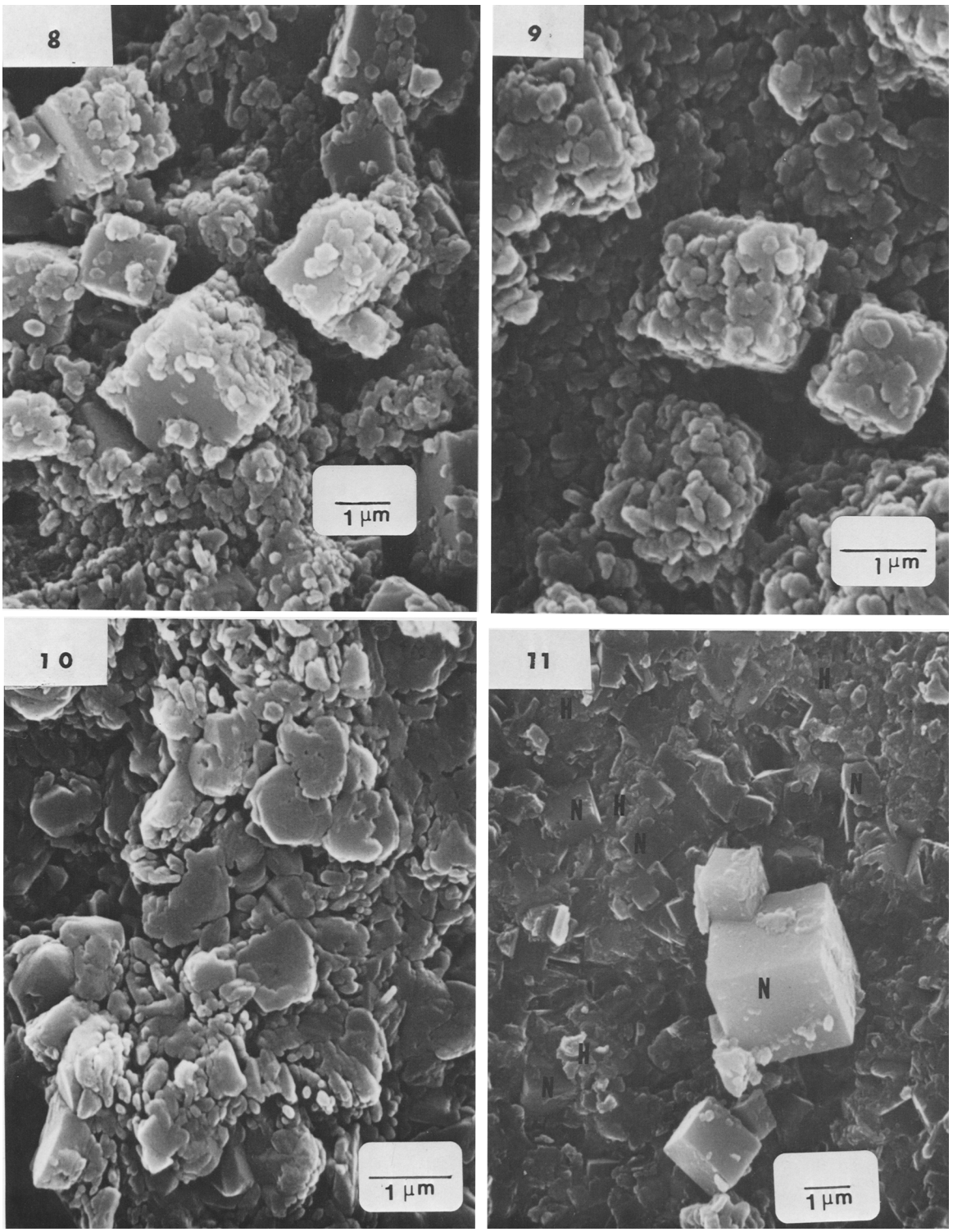

Figure 10. Scanning electron micrograph showing anhedral platelets of gibbsite that were identified by their energy-dispersive X-ray spectra consisting of pure alumina.

Figure 11. Crystal aggregates of natraolunite (N), tightly cemented by microcrystalline hematite (H).

https://doi.org/10.1346/CCMN.1987.0350305 Published online by Cambridge University Press

$$3\,\text{kaolinite} + 2\,Na^+ + 6\,H^+ + 4\,SO_4^{2-} + 9\,H_2O = 2\,\text{natroalunite} + 6\,H_4SiO_4.$$

The equilibrium constant for the above reaction is:

$$K_{eq} = (aH_4SiO_4)^6/(aNa^+)^2 \cdot (aH^+)^6 \cdot (aSO_4^{2-})^4,$$

where pH and the activities of Na^+, SO_4^{2-}, and H_4SiO_4 are the controlling geochemical factors. Depending on these factors, the equilibrium can shift to the right or to the left, kaolinite may convert to natroalunite, or the reversal of the reaction may take place. The stability fields of kaolinite, alunite, gibbsite, muscovite, and K-feldspar at 25°C were reported by Raymahashay (1968). The alunite-kaolinite and alunite-gibbsite phase boundaries in Raymahashay's diagram show that the upper pH limit of alunite stability is 5.5, above which gibbsite or kaolinite is more stable depending on the silica activity. Considering the above geological and geochemical constraints, the following mechanism is proposed for the formation of natroalunite at Matanumad.

Oxidation of pyrite in the Eocene lignite beds and black shales overlying the laterites yielded sulfuric acid and rendered the percolating water acidic. The sodium concentration of the percolating water was probably increased by the alteration of Na-bearing minerals in these sediments. The acidic meteoric water charged with Na^+ moved downwards through the underlying laterite crust along channels, cracks, and other interconnected open pores. The downward-moving acidic water reacted with some of the kaolinite in the laterite crust along its path, and natroalunite precipitated. Thus, some of the kaolinite in the laterite crust was replaced by natroalunite; however, most of the acidic water charged with Na^+ freely percolated downwards and encountered a relatively less permeable layer of saprolitic clay. Low permeability of the saprolitic clay possibly blocked the flow, and acidic water accumulated at the top of the saprolite horizon. By a mechanism similar to the one given by Schoen *et al.* (1974), the acidic water then spread laterally and reacted with kaolinite. A continued supply of fresh sulfuric acid resulted in a complete replacement of nearly all of the kaolinite at the top of the saprolite horizon by natroalunite. The silica released during the alteration of kaolinite to natroalunite was presumably leached away from the laterite profile. The fate of this silica is not known inasmuch as no silica precipitation was found in and around the saprolites. Apparently, the silica concentration did not reach the saturation level for the precipitation of silica.

ACKNOWLEDGMENTS

We thank R. M. Badve, M.A.C.S. Research Institute, Pune, India, for many helpful discussions at the initial stage of the work in India. Special appreciations are also due to B. L. Allen, Texas Tech University, for critically reviewing the manuscript. We express our special thanks to G. Bárdossy, Hungarian Aluminum Company, Budapest, Hungary, and R. B. Hall, U.S. Geological Survey, Denver, Colorado, for reviews that greatly improved the manuscript. Robert I. Botto of Exxon Research and Engineering Company, Baytown, Texas, kindly analyzed the natroalunite sample with plasma atomic emission spectroscopy.

REFERENCES

Biswas, S. K. (1971) Note on the geology of Kutch: *Quart. J. Geol. Mining and Metallurgical Soc. India* **43,** 223–235.

Brophy, G. P., Scott, E. S., and Snellgrove, R. A. (1962) Sulfate Studies II. Solid solution between alunite and jarosite: *Amer. Mineral.* **47,** 112–126.

Cunningham, C. G., Jr. and Hall, R. B. (1976) Field and laboratory tests for the detection of alunite and determination of atomic percent potassium: *Econ. Geol.* **71,** 1596–1598.

Das Gupta, S. K. (1984) Bauxite and aluminum ore resources in India: in *Bauxite,* L. Jacob, Jr., ed., American Institute of Mining, Metallurgical and Petroleum Engineers, Inc., New York, 451–485 pp.

Hemley, J. J., Hostetler, P. B., Gude, A. J., and Mountjoy, W. T. (1969) Some stability relations of alunite: *Econ. Geol.* **64,** 599–613.

Lindsay, W. L. (1979) *Chemical Equilibria in Soils:* Wiley, New York, 449 pp.

Menchetti, S. and Sabelli, C. (1976) Crystal chemistry of the alunite series: Crystal structure refinement of alunite and synthetic jarosite: *Neues Jahrb. Mineral. Monatshefte* **H9,** 406–417.

Moss, A. A. (1958) Alumian and natroalunite: *Mineral Mag.* **31,** 884–885.

Okada, K., Hirabayashi, J., and Ossaka, J. (1982) Crystal structure of natroalunite and crystal chemistry of the alunite group: *Neues Jahrb. Mineral. Monatshefte* **H12,** 534–540.

Ossaka, J., Hirabayashi, J., Okada, K., and Kobayashi, R. (1982) Crystal structure of minamiite, a new mineral of the alunite group: *Amer. Mineral.* **67,** 114–119.

Parker, R. L. (1962) Isomorphous substitution in natural and synthetic alunite: *Amer. Mineral.* **47,** 127–136.

Raymahashay, B. C. (1968) A geochemical study of rock alteration by hot springs in the Paint Pot Hill area, Yellowstone Park: *Geochim. Cosmochim. Acta* **32,** 499–522.

Schoen, R., White, D. E., and Hemley, J. J. (1974) Argillization by descending acid at Steamboat Springs, Nevada: *Clays & Clay Minerals* **22,** 1–22.

Shukla, R. T., Balasubramaniam, K. S., and Madhukara, N. (1983) Paleoenvironment, stratigraphy and genesis of bauxite deposits of Gujarat state, India: in *Proceedings of the 2nd International Seminar on Lateritisation Processes,* A. J. Melfi and A. Carvalho, eds., I.A.G.C., São, Paulo, Brazil, 209–224.

(Received 10 December 1985; accepted 29 August 1986; Ms. 1547)